NASA Technical Memorandum 80142

EFFECT OF OUTBOARD VERTICAL-FIN POSITION AND ORIENTATION ON THE LOW-SPEED AERODYNAMIC PERFORMANCE OF HIGHLY SWEPT WINGS

Vicki S. Johnson and Paul L. Coe, Jr.

(NASA-TM-80142) EFFECT OF OUTBOARD VERTICAL-FIN POSITION AND ORIENTATION ON THE LOW-SPEED AERODYNAMIC PERFORMANCE OF HIGHLY SWEPT WINGS (NASA) 30 p HC A03/MF A01 CSCL 01A

N79-32158

Unclas G3/02 35814

September 1979

National Aeronautics and Space Administration

Langley Research Center
Hampton, Virginia 23665

SUMMARY

A theoretical study has been conducted to determine the potential low-speed performance improvements which can be achieved by altering the position and orientation of the outboard vertical fins of low-aspect-ratio highly swept wings. As expected, the results of the study show that the magnitude of the performance improvements is solely a function of the span-load distribution. Both the vertical-fin-chordwise position and toe angle provided effective means for adjusting the overall span-load distribution.

INTRODUCTION

The National Aeronautics and Space Administration is currently investigating the aerodynamic characteristics of advanced aircraft concepts which are intended to cruise efficiently at supersonic speeds (see refs. 1 and 2). Such configurations employ a highly swept planform, which is twisted and cambered to achieve the desired high level of cruise aerodynamic efficiency. These configurations typically include outboard vertical fins which are intended to provide directional stability, but which (when properly aligned in the cruise condition) can be shown to produce a forward component of force which is in excess of the additional skin friction drag, and hence the inclusion of the outboard vertical fins provides a net supersonic performance gain.

The necessary emphasis on optimizing these conceptual wing--outboard-vertical-fin designs for the supersonic cruise condition has resulted in aircraft concepts which would exhibit relatively poor low-speed performance in typical takeoff and landing situations. Previous efforts directed towards providing these concepts with improved low-speed performance have been limited to studies of the leading-and trailing-edge systems (see, for example refs. 3 and 4).

The present study, which utilizes a planar vortex-lattice theoretical model of the highly swept-wing vertical-fin configuration, is intended to determine the effect on aerodynamic performance of changes in vertical-fin chordwise position and toe and cant angle.

SYMBOLS

Force coefficients are referred to the wind system of axes.

A	wing aspect ratio, b^2/S
b	wing span, m (ft)
c	local wing chord, m (ft)
c_{avg}	average wing chord, S/b, m (ft)
C_{D_i}	induced drag coefficient, Induced drag/qS
C_L	lift coefficient, Lift/qS
c_ℓ	section-lift coefficient
c_y	section side-force coefficient
e	span efficiency factor, $C_L{}^2/\pi A C_{D_i}$
M	Mach number
q	free-stream dynamic pressure, Pa (lbf/ft^2)
S	wing area, m^2 (ft^2)
x	chordwise distance of the leading edge of the fin behind the leading edge of the wing, m (ft)
y	spanwise distance measured from wing centerline, m (ft)
z	vertical fin ordinate, origin at wing vertical-fin intersection, positive upwards, m (ft)
α	angle of attack, deg
δ_f	trailing-edge flap deflection, positive trailing edge down, deg
σ	sidewash angle at vertical fin, positive outwards, deg
τ	toe angle of vertical fin, positive toe-in, deg
λ	cant angle of vertical fin, positive outwards, deg

Subscripts:

o	indicates condition without vertical fin

CONFIGURATIONS SIMULATED

The study was conducted for the two configuration geometries shown in figure 1 and defined in references 5 and 6. These geometries (referred to as configuration A and configuration B) were simulated using the planar vortex-lattice computer program described in reference 7. Configuration A included both twist and camber (see ref. 5) and a planar fuselage representation. Configuration B was untwisted and uncambered and did not incorporate a fuselage. Figure 2 depicts schematically the vortex-lattice paneling schemes used to represent the configuration geometries.

RESULTS AND DISCUSSION

In the present study, a relative span efficiency factor, e/e_o, is introduced where

$$\frac{e}{e_o} = \frac{\text{span efficiency factor - wing with outboard vertical fin}}{\text{span efficiency factor - wing without outboard vertical fin}}$$

This factor is introduced in an attempt to reduce the dependence of the numerical results on the particular paneling scheme and vortex spacing used. It is acknowledged, however, that changes in either the paneling scheme or the vortex spacing will affect the values of e/e_o to some extent. Therefore, values of e/e_o should be considered as a qualitative figure of merit, which is introduced to assess the relative effect on performance of changes in vertical-fin chordwise position and vertical-fin toe and cant angles.

Effect of Vertical-Fin Chordwise Position

Figure 3 shows the effect of varying the chordwise position of the vertical fin on the relative span efficiency factor, e/e_o. As can be seen, changes in chordwise position result in modest changes in span efficiency; however, the most interesting point to be noted is the different trend exhibited by the results for configurations A and B. For configuration A, the results indicate an increase in span efficiency factor can be achieved by moving the outboard-vertical fin forward relative to the wing. By contrast, the results for configuration B indicate that the maximum span efficiency can be achieved by moving the outboard-vertical fins rearward to approximately $x/c = 0.2$. It should be further noted that e/e_o is a reasonably smooth function of x/c, indicating that the computational results are fairly insensitive to the relative alignment of the bound vortices representing the wing and vertical fin.

Inasmuch as the span efficiency factor is a function of the span-load distribution, some insight into the preceding differing trends of e/e_o can be afforded by considering this quantity. Figure 4 presents the calculated optimum span-load distribution for configuration A. The optimization seeks a minimum induced drag using a Trefftz plane far-field drag computation (see ref. 7). Although for a planar wing this result is accomplished by obtaining a uniform downwash at downstream infinity, the present nonplanar solution utilizes Lagrange multipliers to minimize the induced drag. Also presented in figure 4 are the calculated span-load distributions for configuration A having vertical fins located at x/c = 0 and ± 0.2. The results show that for this configuration moving the outboard-vertical fins forward produces an increased inward load on the vertical fins, a slightly increased span load on the portion of the wing inboard of the vertical fins, and a slightly reduced span load on the outboard wing panel. The net result being that, for the values of x/c investigated, the condition with x/c = -0.2 results in a span-load distribution, particularly the vertical-fin side-force load distribution, which is closest to the optimum, and hence, exhibits the higher span efficiency factor as shown in figure 3.

Figure 5 presents the optimum span-load distribution and the span-load distribution for the condition of x/c = 0 and ± 0.2 for configuration B. As can be seen, moving the outboard vertical fin of configuration B aft to x/c = 0.2 results in a reduction of the inwardly directed load on the vertical fins, a reduction in the span load inboard of the vertical fins, and an increase in span load on the outboard wing panel. This trend is in complete agreement with the results for configuration A, however, in this case the reduced vertical-fin loads result in a condition which more closely approaches the optimum. Therefore, it can be concluded that the eff ct of vertical-fin chordwise position on the span efficiency factor is simply a function of how closely the optimum span-load distribution can be approximated.

Recognizing that the load on the vertical fin is a function of the local angle of attack (e.g. sidewash in the case of a vertical surface) leads to an understanding of the fluid mechanism responsible for the preceding results. Figure 6 presents the calculated sidewash distribution along the vertical fin. As can be seen, moving the vertical fin forward would produce an increased resultant angle of attack and hence an increase in the inward vertical-fin load. Correspondingly, moving the vertical fin aft would produce a reduction in resultant angle of attack and a reduction in the inward vertical-fin load. The change in the span-load distribution of the wing, which is observed to accompany the change in vertical-fin load, simply results from a change in circulation (see fig. 7). An increase in the inward vertical-fin load would occur with an increase in the circulation around the vertical fin. As shown by the sketch of figure 7, the increased circulation would tend to reinforce the circulation (and increase the span load) over the inboard portion of the wing, while tending to oppose the circulation (and reduce the span load) over the outboard portion of the wing.

Effect of Vertical-Fin Toe Angle

The effect of vertical-fin toe angle, τ, on the relative span efficiency factor of configuration A is presented in figure 8. As can be seen, an angle corresponding to approximately $\tau = 2^\circ$ results in a maximum span efficiency. This result is simply related to the span-load distribution as previously discussed and is totally consistent with the preceding result which showed an increased span efficiency achieved for this configuration by moving the vertical fins forward. (Both toe-in and forward placement of the vertical fin result in an increased angle of attack for the vertical fin.) The result is further illustrated by the span-load distributions presented in figure 9 for several values of vertical-fin toe angle. As would be expected, $\tau = 2^\circ$, which results in the highest span efficiency factor, also results in a span-load distribution most nearly approaching the optimum.

Effect of Vertical Fin Cant Angle

The effect of vertical fin cant angle, λ, on the relative span efficiency factor of configuration A is presented in figure 10. The results are presented for the configuration with the vertical fin located at $x/c = 0$ and $\tau = 0^\circ$. The results presented show that there is a modest effect of cant angle on performance and that the effect is favorable for positive cant angles and unfavorable for negative angles. This result is simply related to the inward direction of the force acting on the vertical fin. For positive values of λ, a component of the vertical-fin load is acting in the positive lift direction and, hence, results in an increased span efficiency factor. Correspondingly, for negative values of λ, a component of the vertical-fin load is directed in the negative lift direction and, as expected, reduces the span efficiency factor.

Effect of Trailing-Edge Flap Deflection

The results of the preceding sections have shown that the improvements in span efficiency, which are provided by vertical-fin chordwise position and toe angle, are a direct result of such configuration variables providing a more favorable span-load distribution. In order to more clearly illustrate this point, the trailing-edge flap system sketched in figure 11 was subjected to a continuously variable deflection in an attempt to approximate the optimum the span-load distribution. The trailing-edge deflection schedule selected for study is presented in figure 12, and the corresponding span-load distribution is presented in figure 13. As can be seen, the scheduled trailing-edge flap system provides the configuration with a load distribution which is a reasonable approximation to the optimum. With the trailing-edge deflection incorporated into the theoretical model, the effect of vertical-fin chordwise position and vertical-fin toe angle on the span efficiency factor is reconsidered. The results are presented in figures 14 and 15, respectively, and show that variations in x/c and τ (from the condition of $x/c = 0$ and $\tau = 0°$) result in reductions in the span efficiency factor. These results are, of course, expected as the span-load distribution for the configuration with the scheduled trailing-edge flaps (and having $x/c = 0$ and $\tau = 0°$) has been shown to be nearly optimum.

CONCLUSION

A theoretical study has been conducted to determine the potential low-speed performance improvements which can be achieved by altering the position and orientation of the outboard vertical fins of low-aspect-ratio highly swept wings. As expected, the results of the study show that the magnitude of the performance improvements is solely a function of the span-load distribution. Both the vertical-fin-chordwise position and toe angle provided effective means for adjusting the overall span-load distribution.

REFERENCES

1. Robins, A. Warner; Morris, Odell A.; and Harris, Roy V., Jr.: Recent Results in the Aerodynamics of Supersonic Vehicles. J. Aircraft, vol. 3, 1966, pp. 573-577

2. Robins, A. Warner; Lamb, Milton; and Miller, David S.: Aerodynamic Characteristics at Mach Numbers of 1.5, 1.8, and 2.0 of Blended Wing-Body Configuration With and Without an Integral Canard. NASA TP 1427, 1979

3. Coe, Paul L., Jr.; and Weston, Robert P.: Effects of Wing Leading-Edge Deflection on the Low-Speed Aerodynamic Characteristics of a Low-Aspect-Ratio Highly Swept Arrow-Wing Configuration. NASA TM 78787, 1978

4. Coe, Paul L., Jr.; and Huffman, Jarrett K.: Influence of Optimized Leading-Edge Deflection and Geometric Anhedral on the Low-Speed Aerodynamic Characteristics of a Low-Aspect-Ratio Highly Swept Arrow-Wing Configuration. NASA TM 80083, 1979

5. Staff, Hampton Technical Center, LTV Aerospace Corporation: Advanced Supersonic Technology Concept Study Reference Characteristics. NASA CR 132374, 1973

6. Manro, Marjorie E.; Manning, Kenneth J. R.; Hallstaff, Thomas H.; and Rogers, John T.: Transonic Pressure Measurements and Comparison of Theory to Experiment for an Arrow-Wing Configuration--Summary Report. NASA CR 2610, 1976

7. Tulinius, J.: Unified Subsonic, Transonic, and Supersonic NAR Vortex Lattice. Rep. TFD-72-253, Rockwell International Corporation, 1972

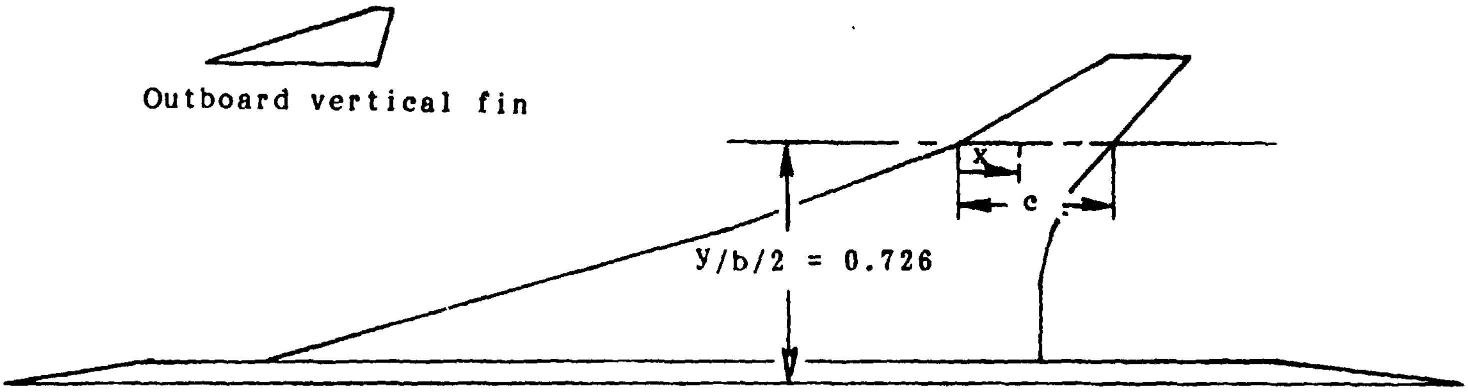

(a) Planform geometry for wing of reference 5 (Configuration A)

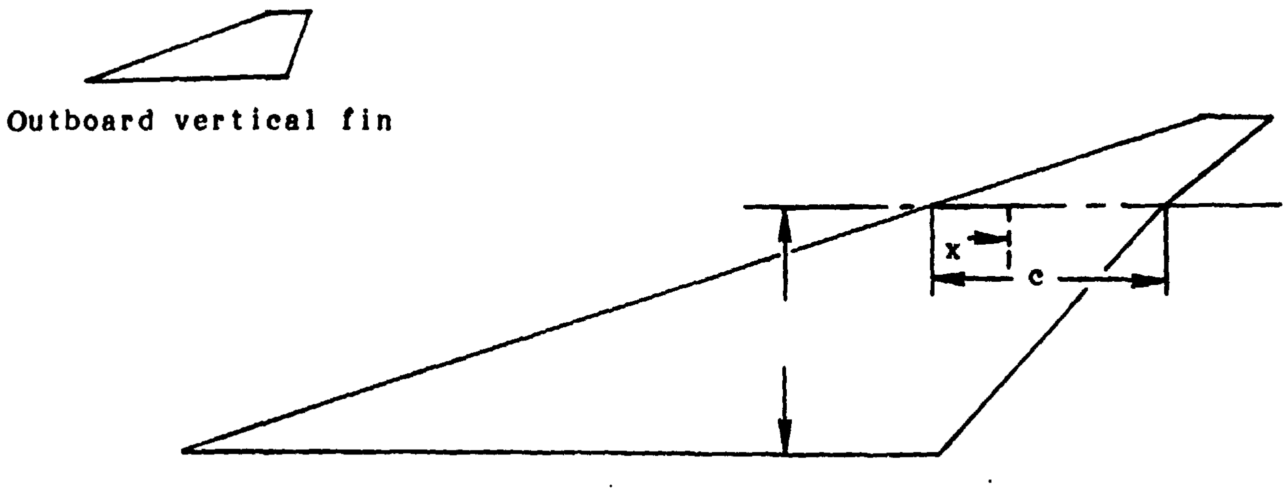

(b) Planform geometry for wing of reference 6 (Configuration B)

Figure 1.- Planform geometries of configurations simulated.

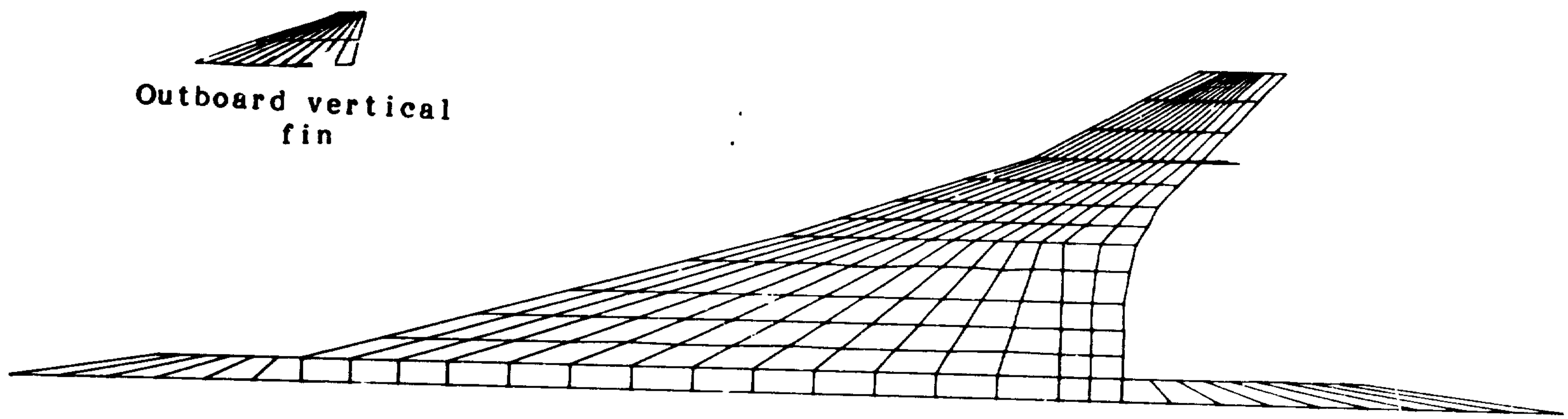

(a) Paneling scheme used to simulate Configuration A

Figure 2.- Paneling schemes used in present study of wing geometries.

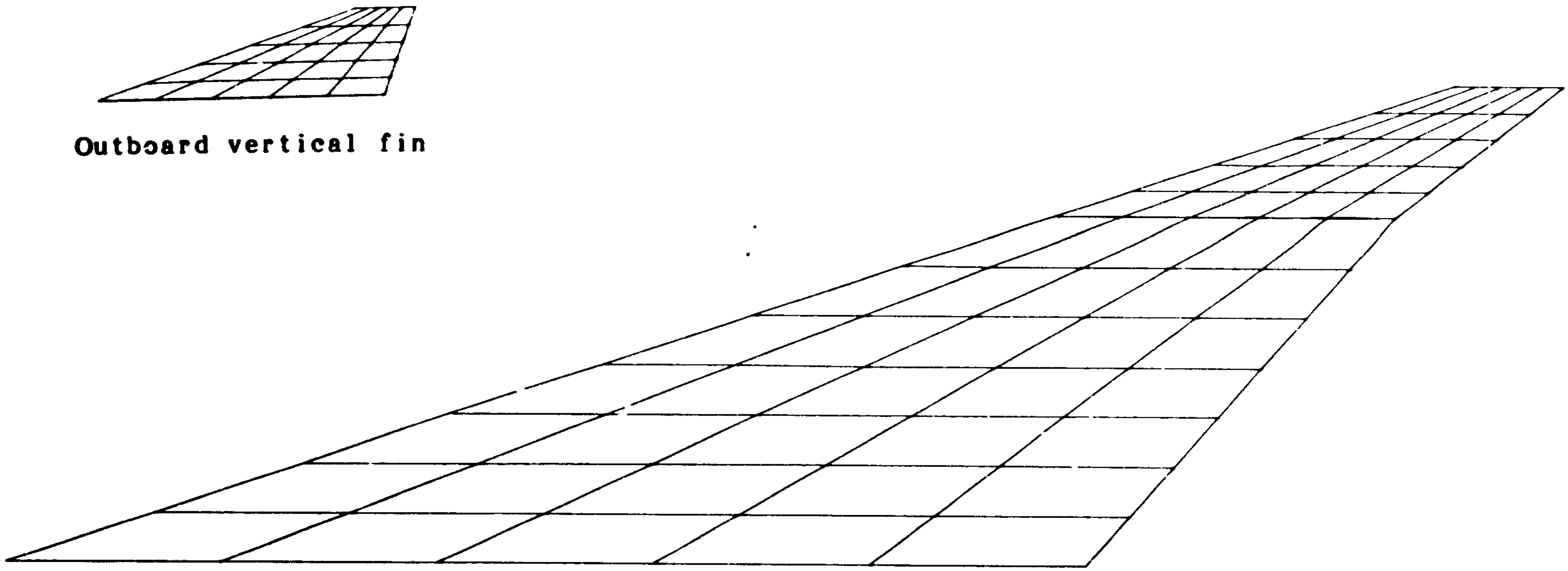

(b) Paneling scheme used to simulate Configuration B
Figure 2.- Concluded.

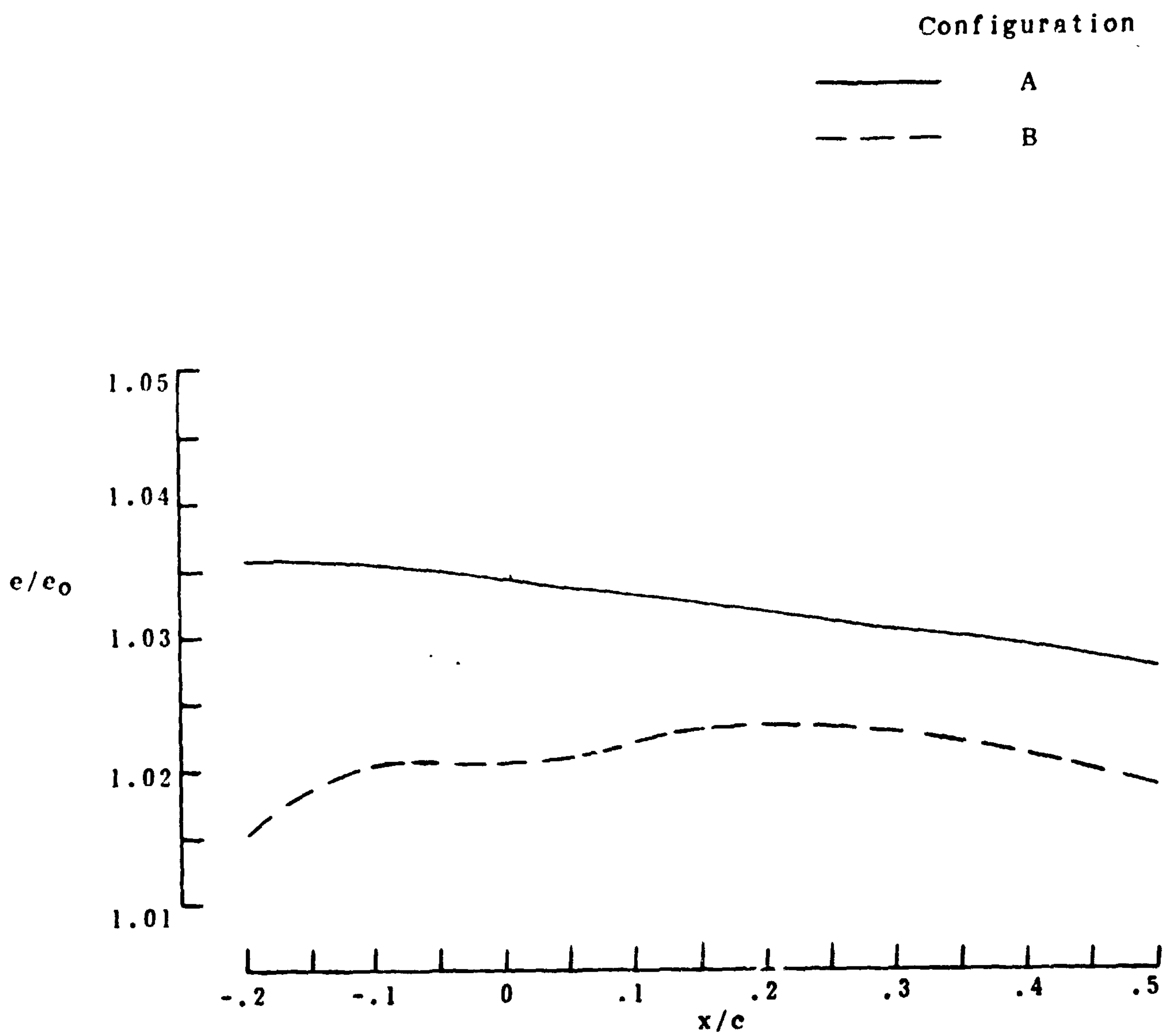

Figure 3.- Effect of vertical-fin chordwise position on relative span efficiency. $\alpha = 10°$, M = 0.

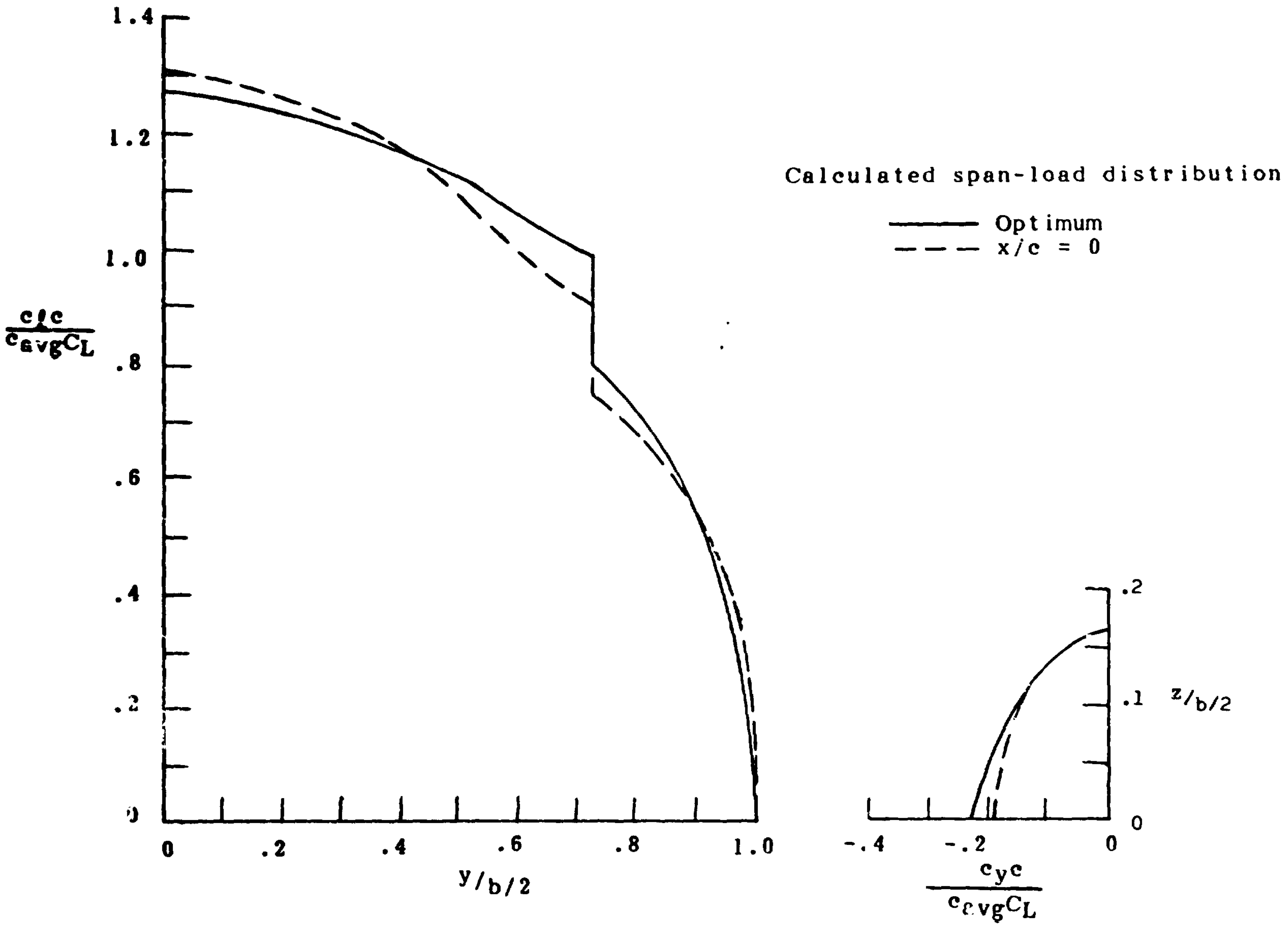

(a) Vertical fin at x/c = 0

Figure 4.- Comparison of optimized span-load distribution with span-load distribution for different values of x/c. Configuration A, $\alpha = 10°$.

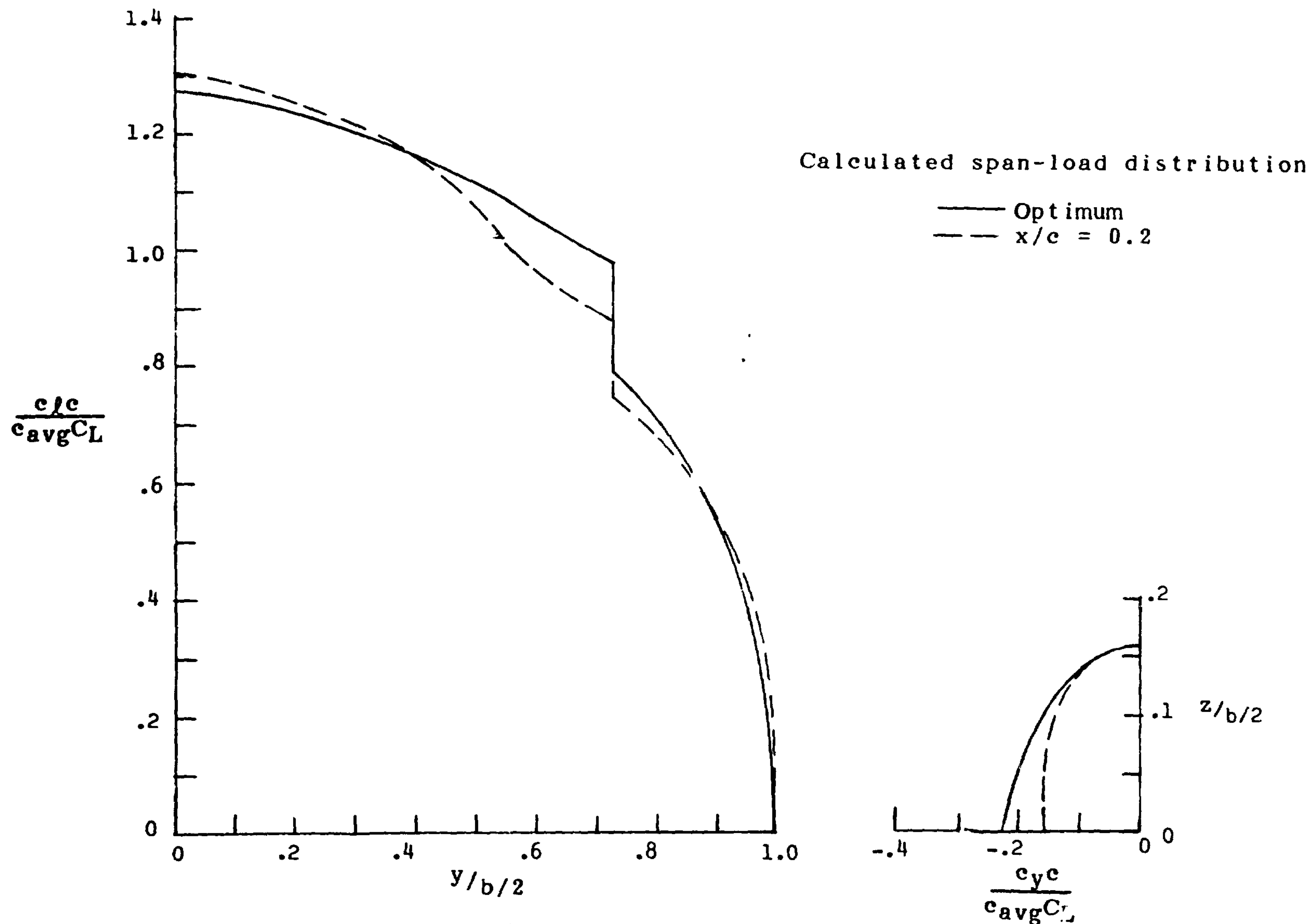

(b) Vertical fin at x/c = 0.2

Figure 4.- Continued.

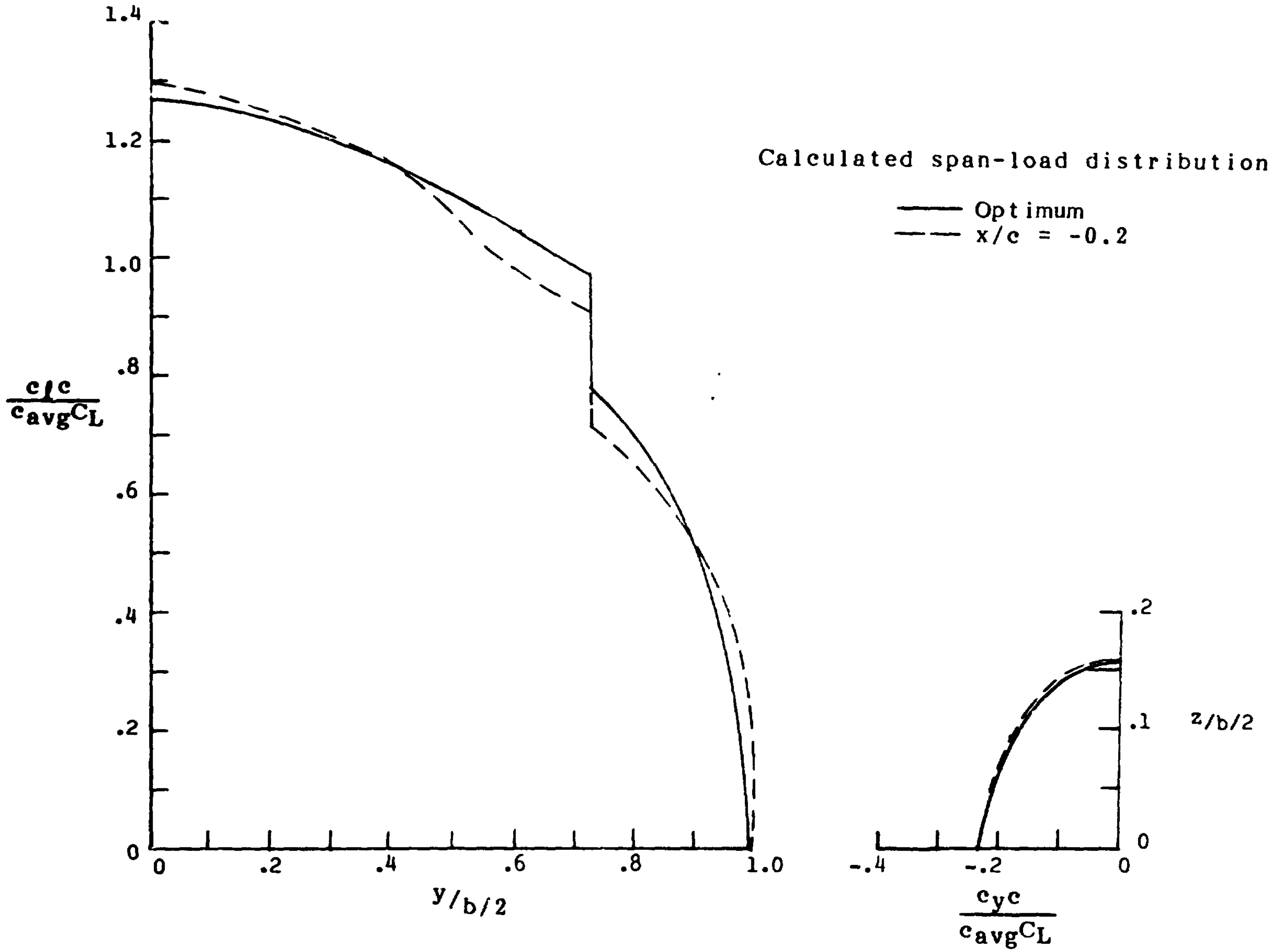

(c) Vertical fin at x/c = -0.2

Figure 4.- Concluded.

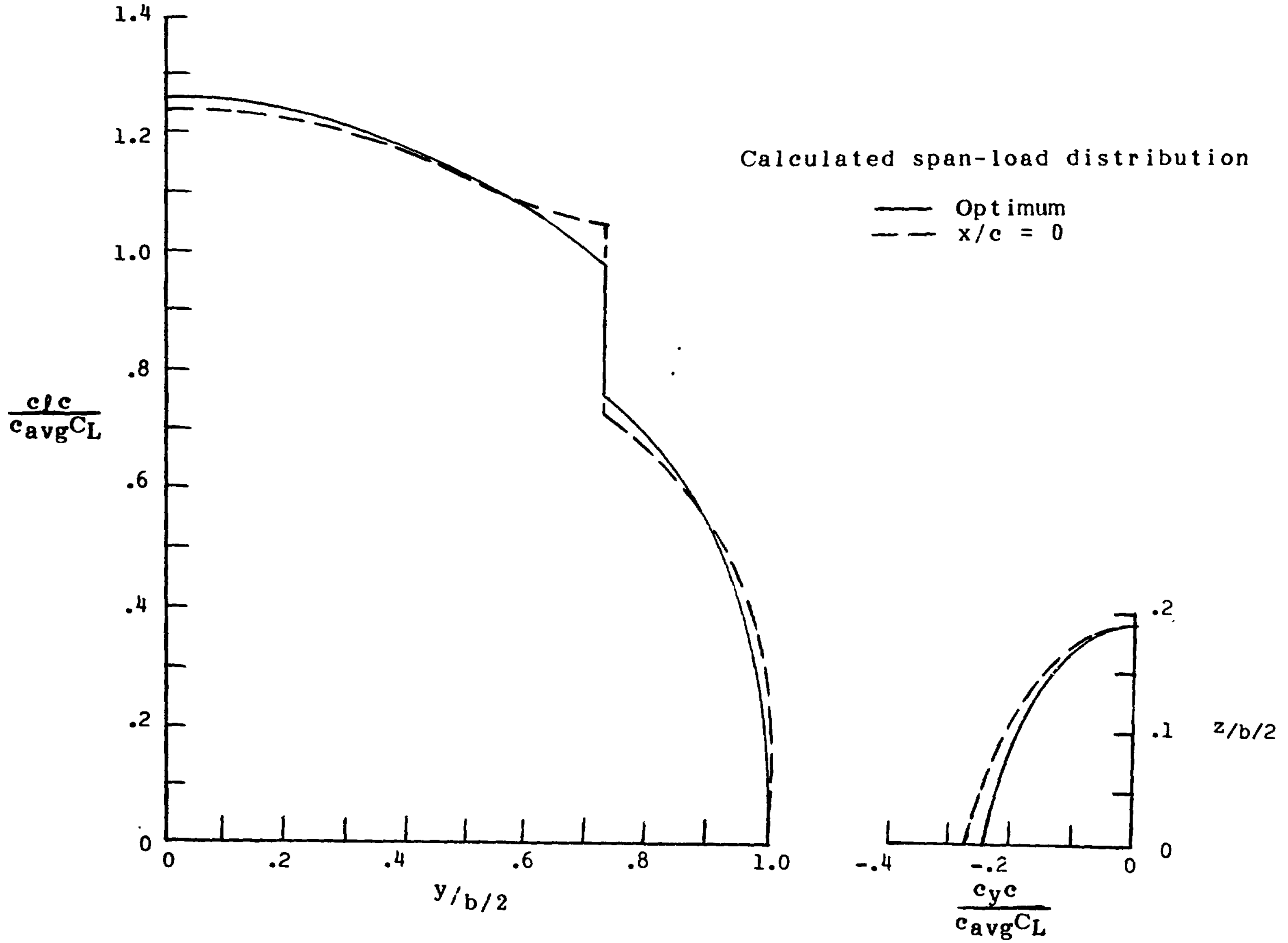

(a) Vertical fin at x/c = 0

Figure 5.- Comparison of optimized span-load distribution with span-load distribution for different values of x/c. Configuration B, $\alpha = 10°$.

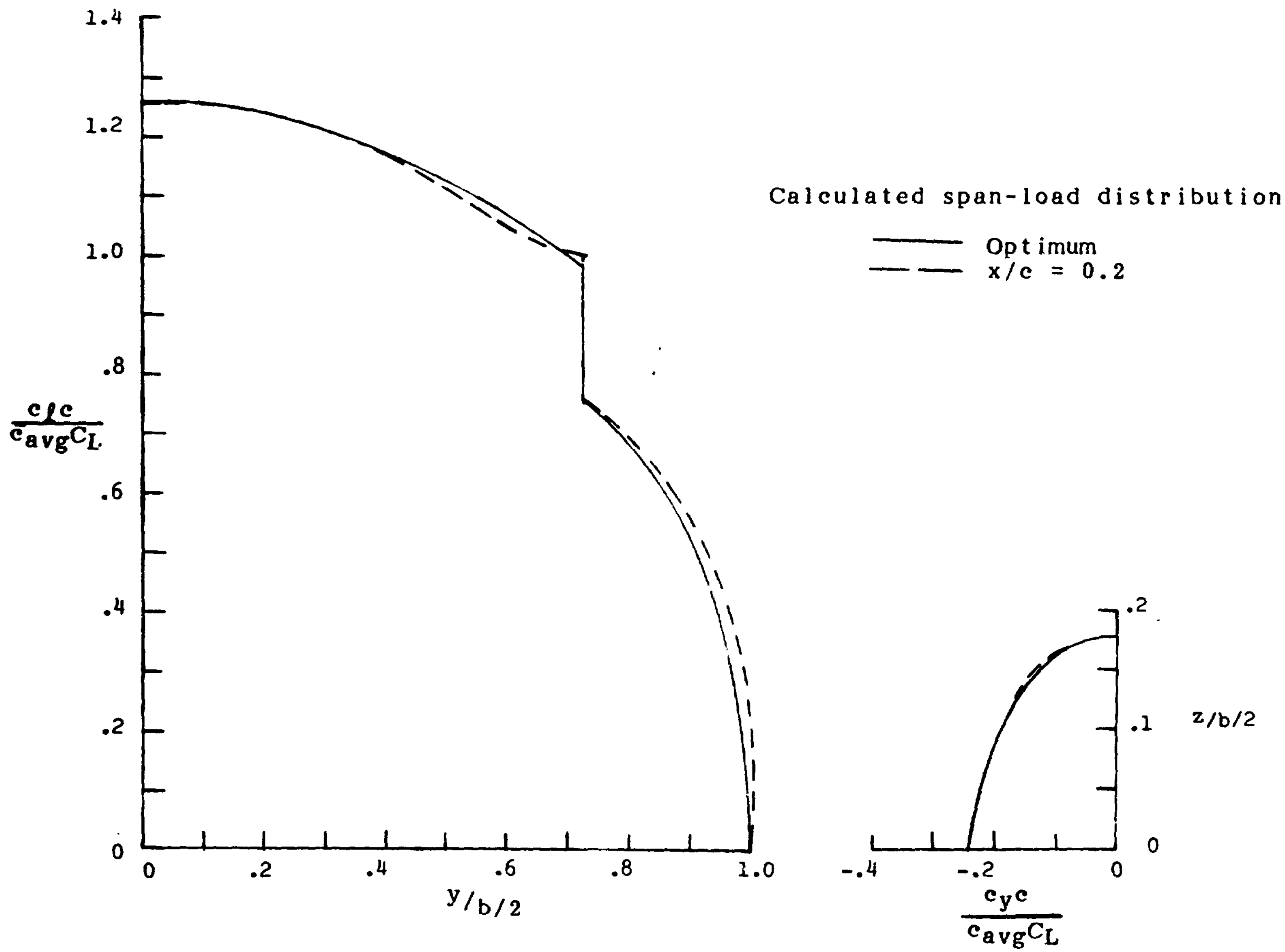

(b) Vertical fin at x/c = 0.2
Figure 5.- Continued.

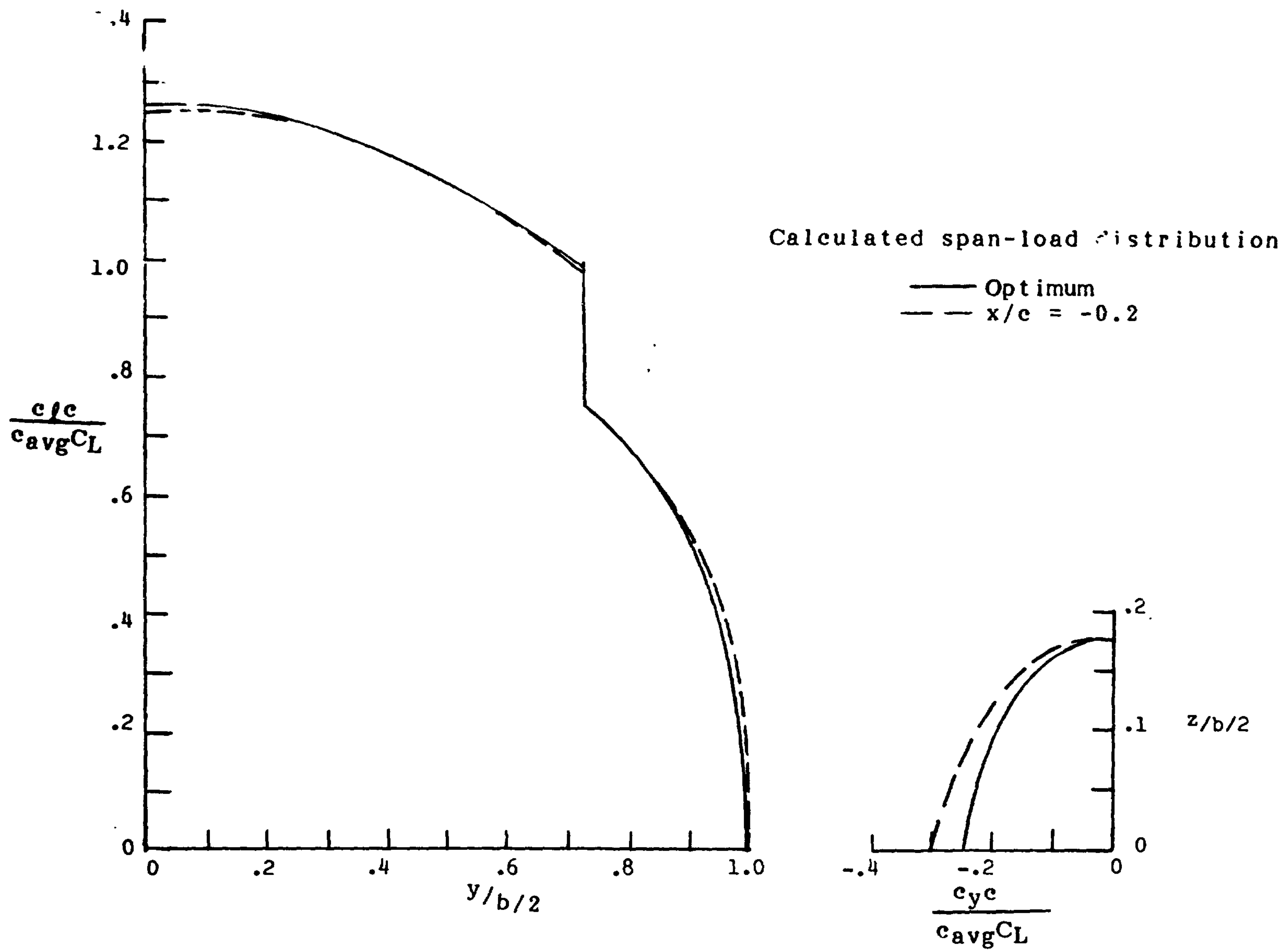

(c) Vertical fin at $x/c = -0.2$
Figure 5.- Concluded.

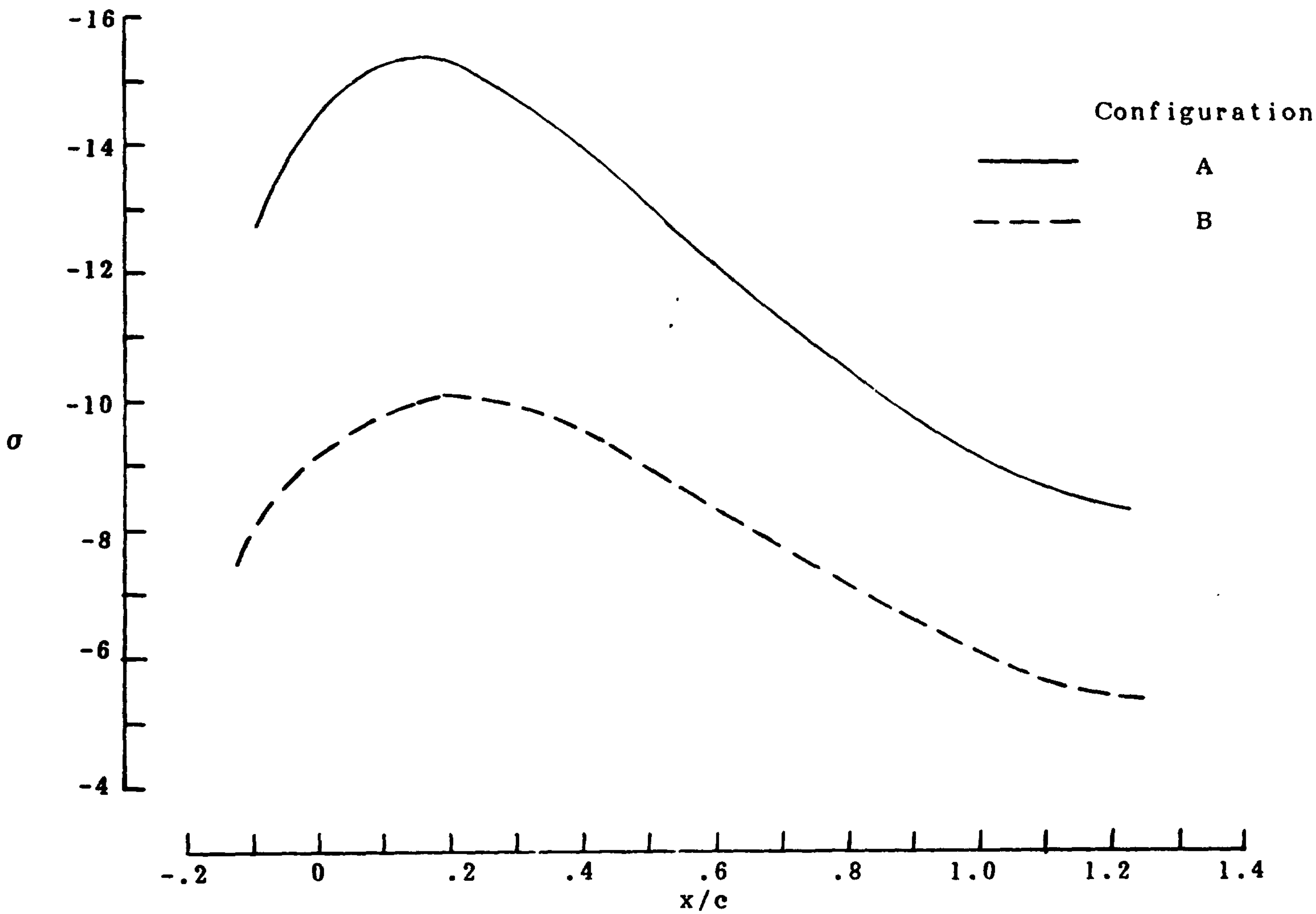

Figure 6.- Sidewash distribution along vertical fin.

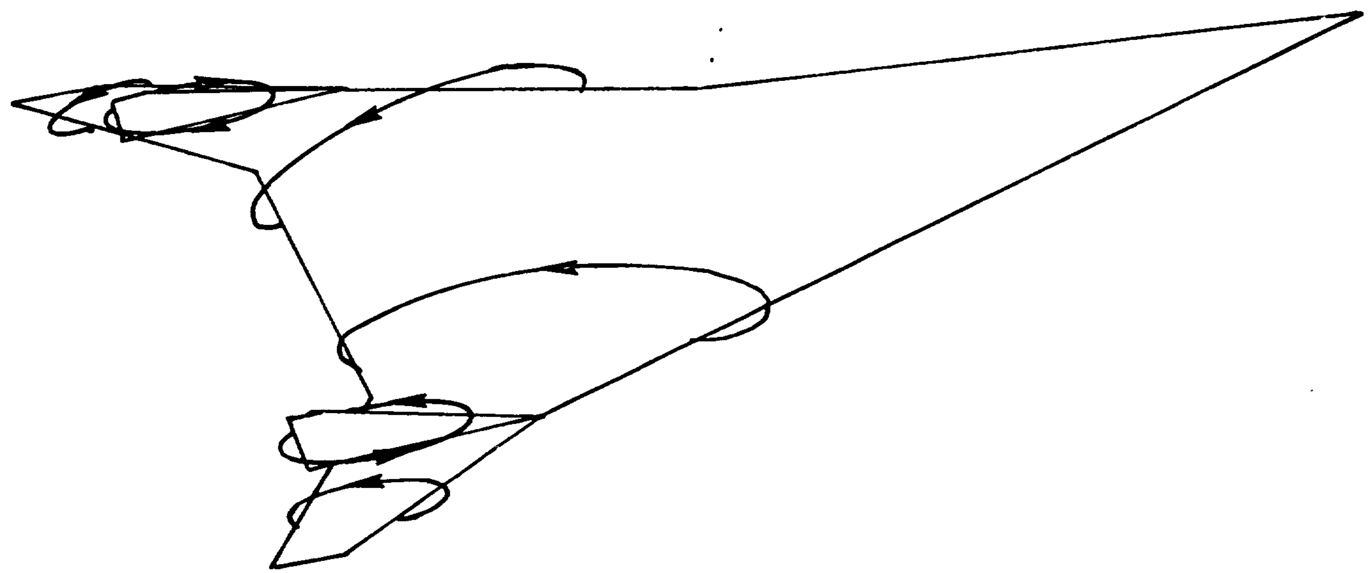

Figure 7.- Sketch showing direction of circulation vectors.

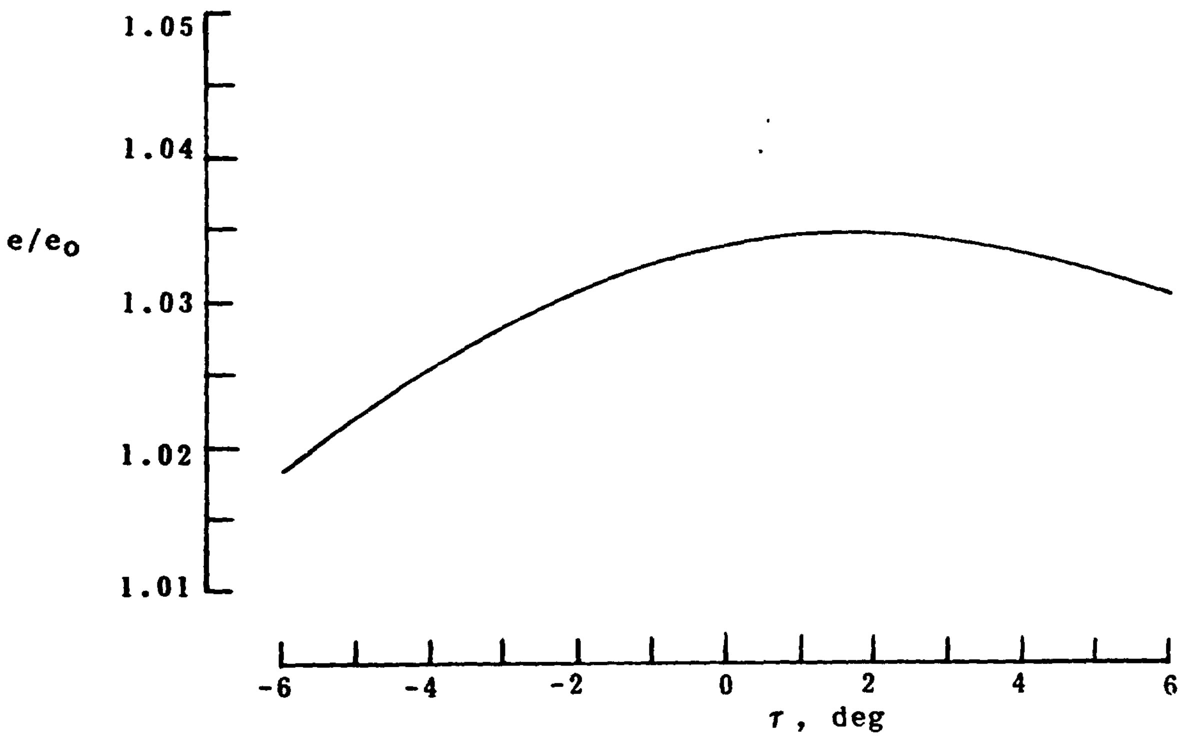

Figure 8.- Effect of vertical-fin toe angle on relative span efficiency factor. Configuration A, vertical fin at $x/c = 0$, $\alpha = 10°$.

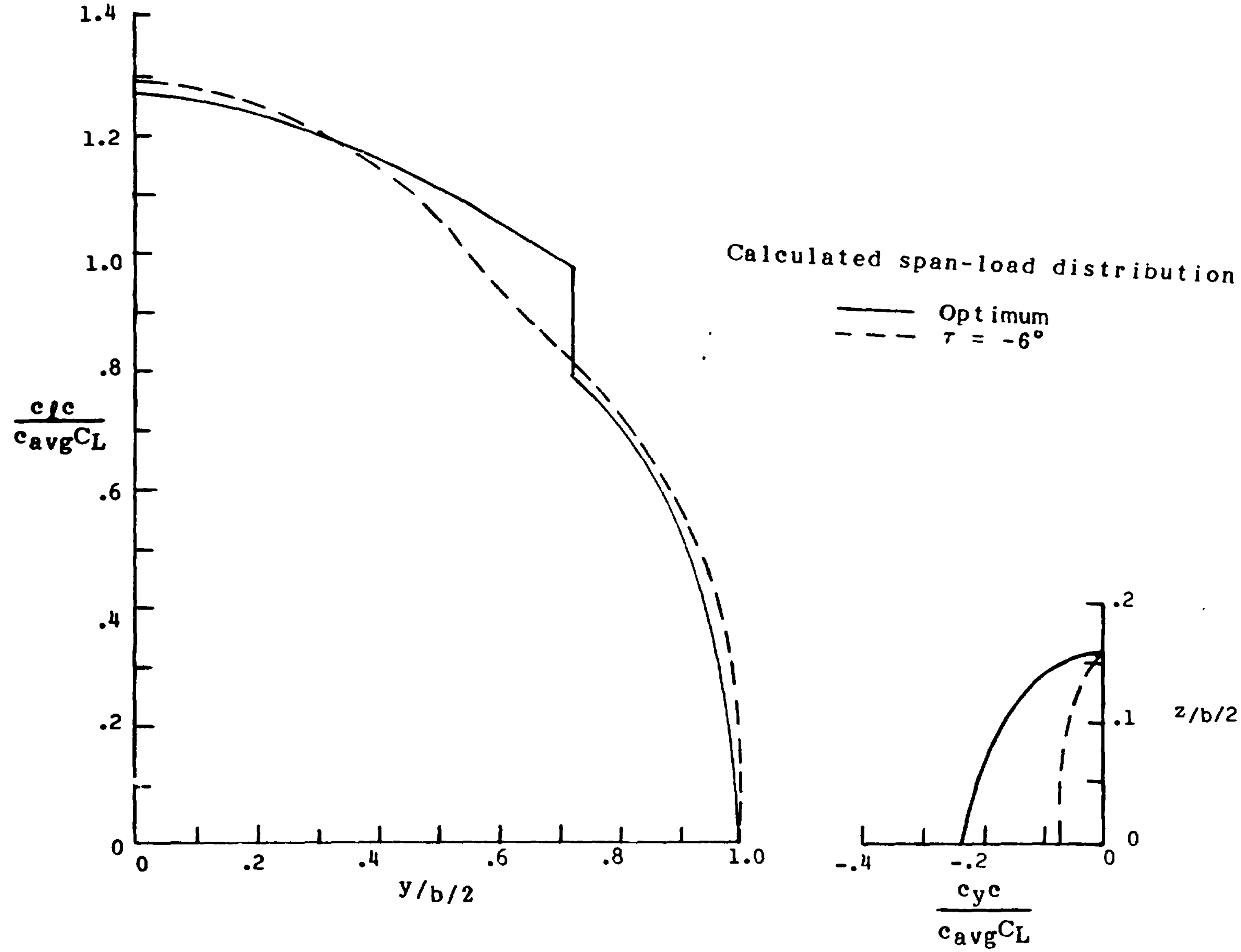

(a) $\tau = -6°$

Figure 9.- Effect of toe angle on span-load distribution. Configuration A, $x/c = 0$, $\alpha = 10°$.

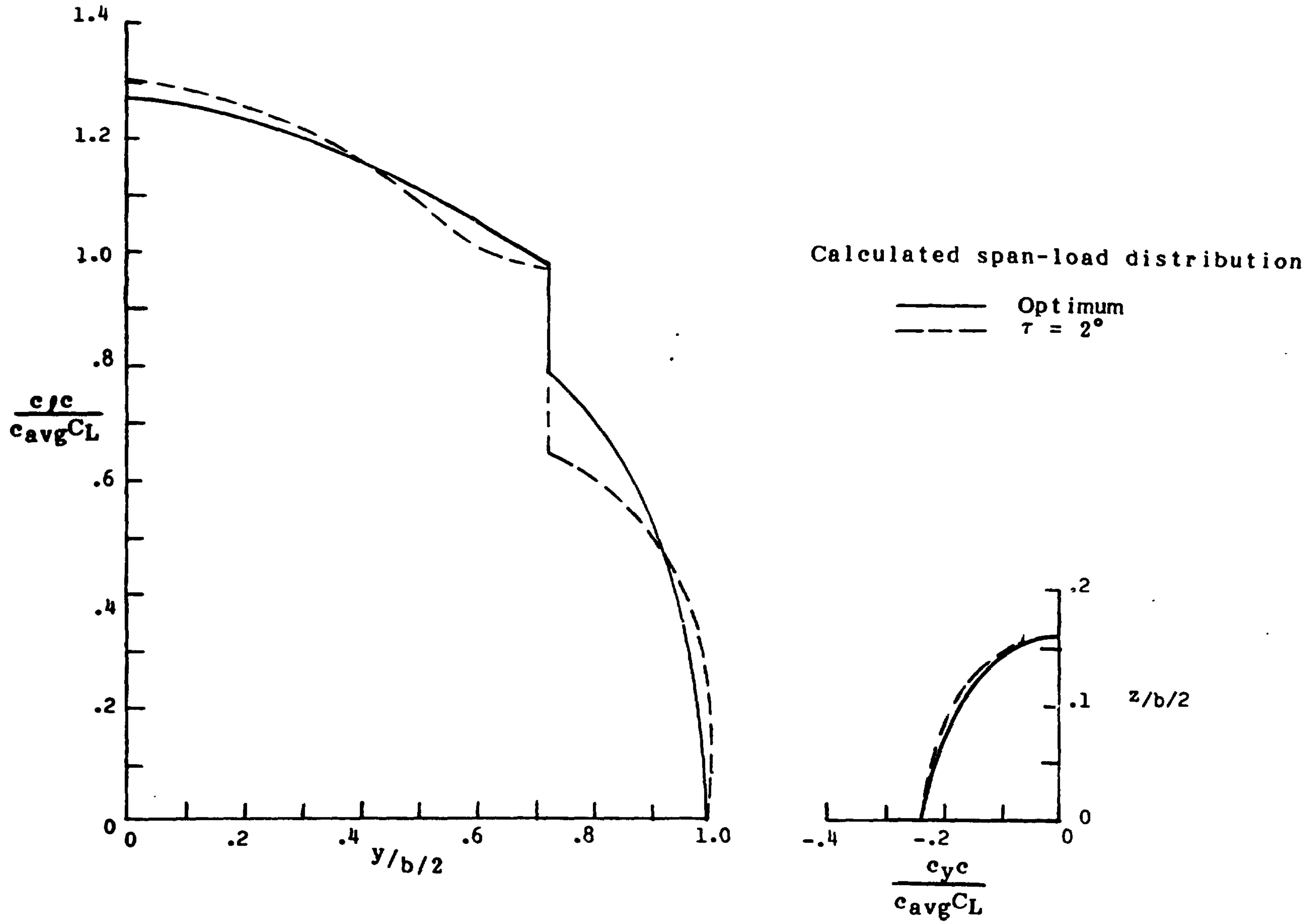

(b) τ = 2°
Figure 9.- Continued.

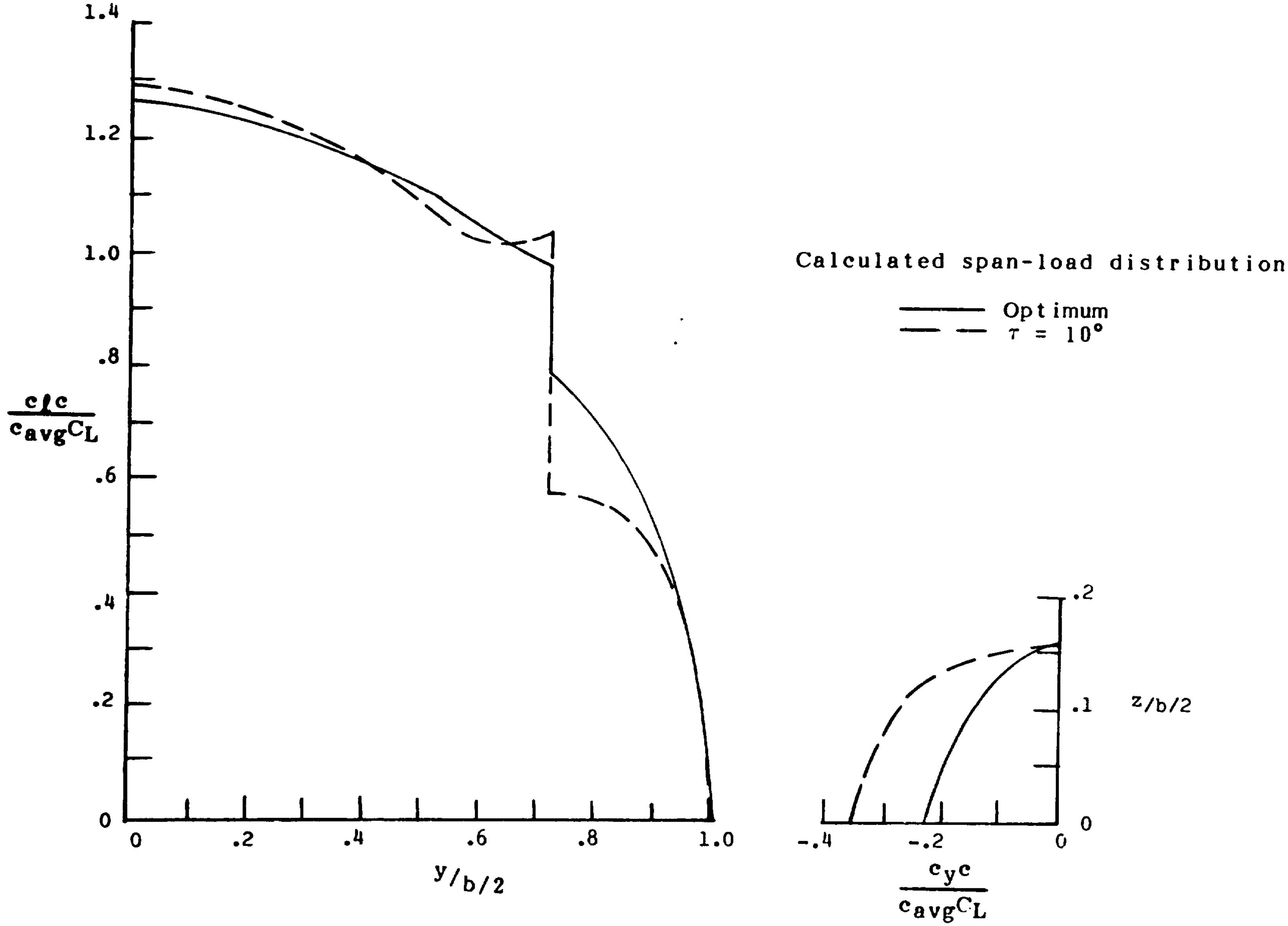

(c) $\tau = 10°$
Figure 9.- Concluded.

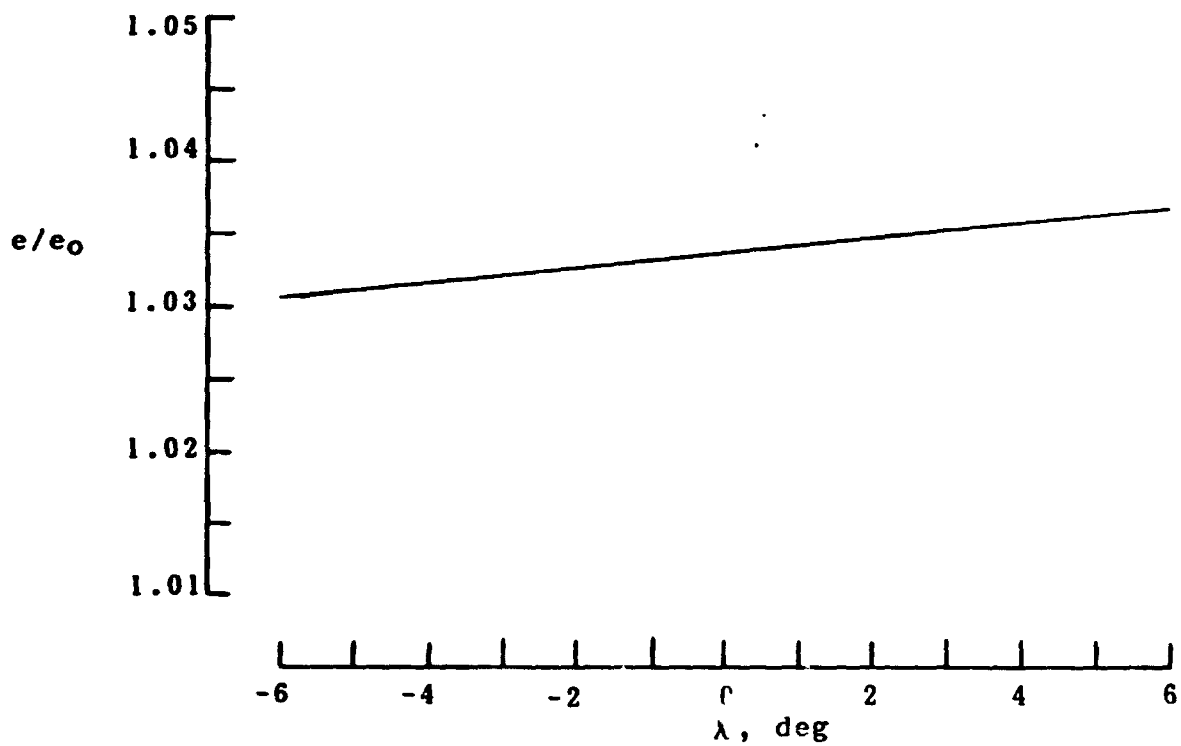

Figure 10.- Effect of vertical-fin cant angle on relative span-efficiency factor. Configuration A, vertical fin at $x/c = 0$, $\tau = 0°$, $\alpha = 10°$.

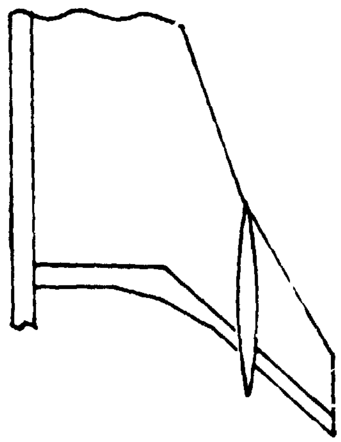

Figure 11.- Trailing-edge flap geometry for Configuraton A.

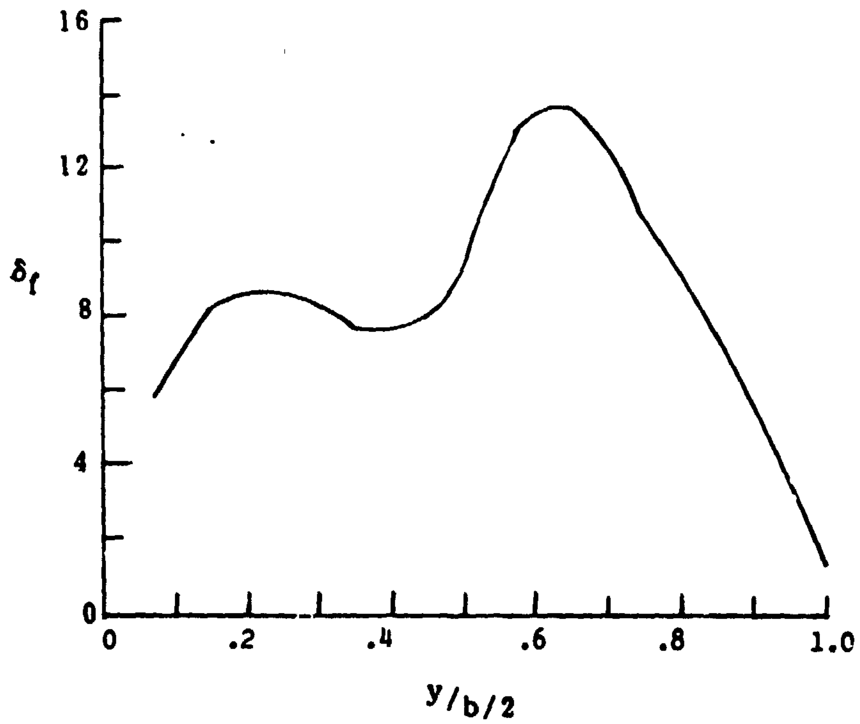

Figure 12.- Schedule for continuously variable trailing-edge deflection, Configuration A.

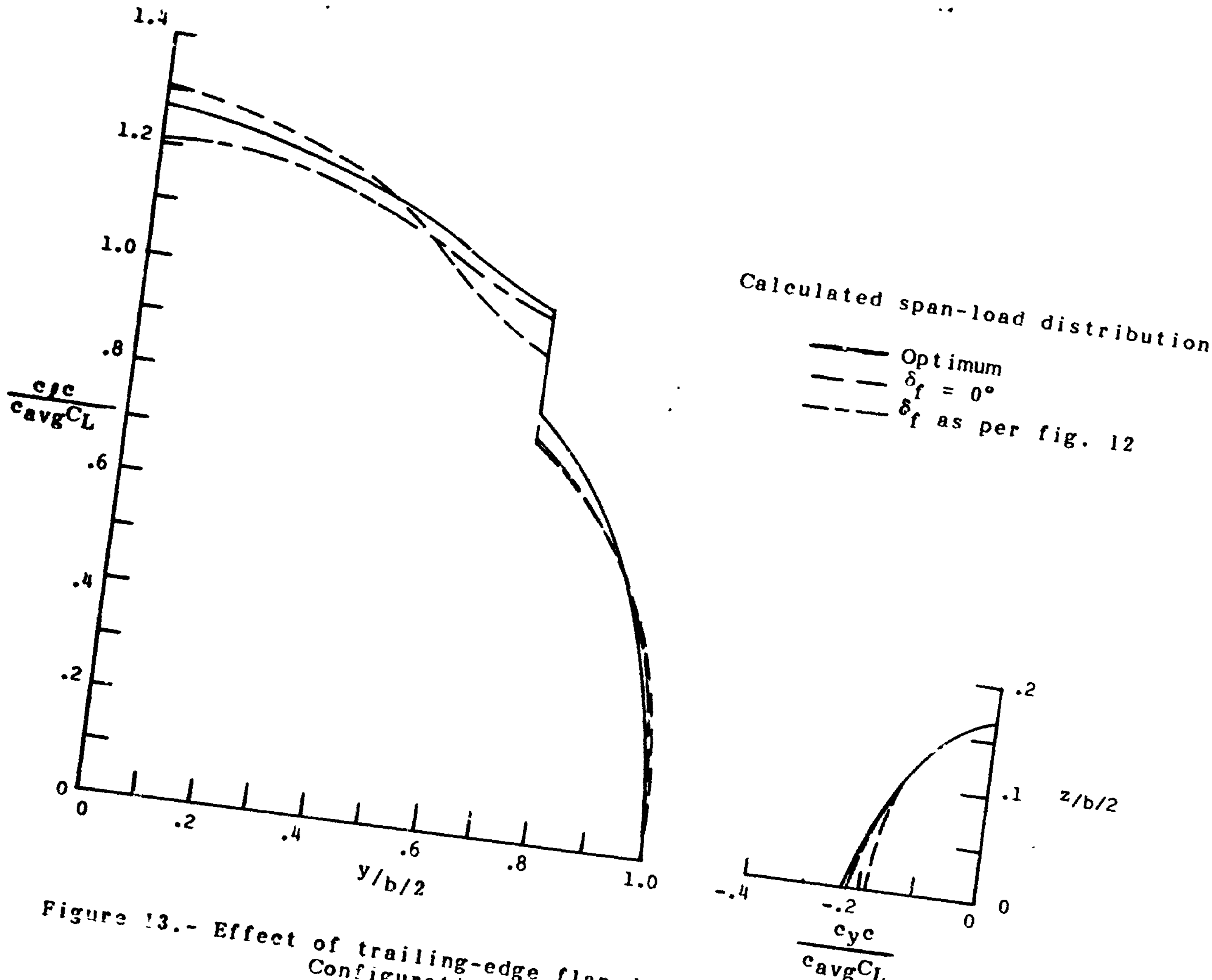

Figure 13.- Effect of trailing-edge flap deflection on span-load distribution. Configuration A, $x/c = 0$, $\tau = 0°$, $\lambda = 0°$.

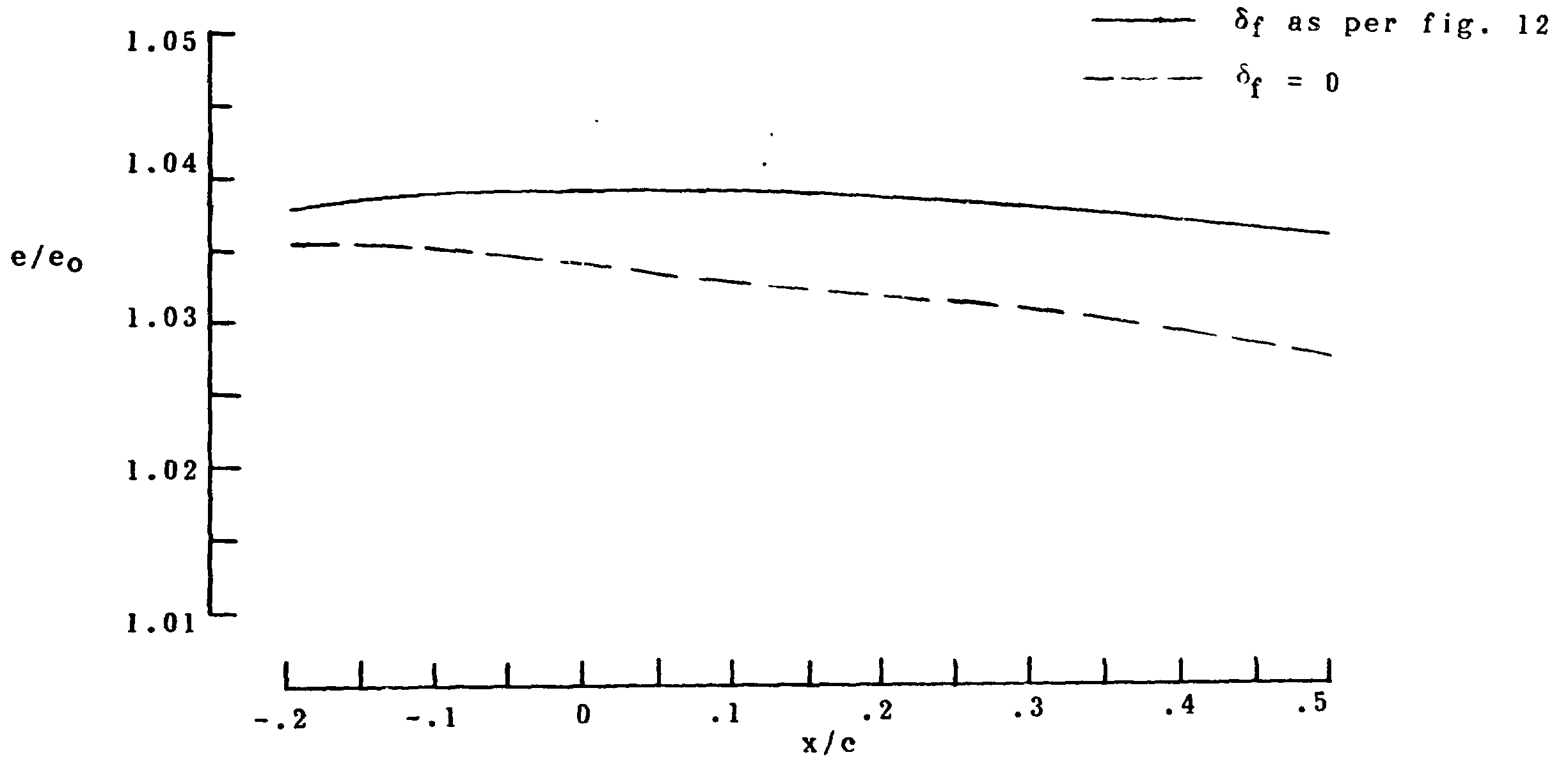

Figure 14.- Effect of vertical-fin chordwise location on relative span-efficiency factor. Configuration A, $\tau = 0°$, $\lambda = 0°$, $\alpha = 10°$.

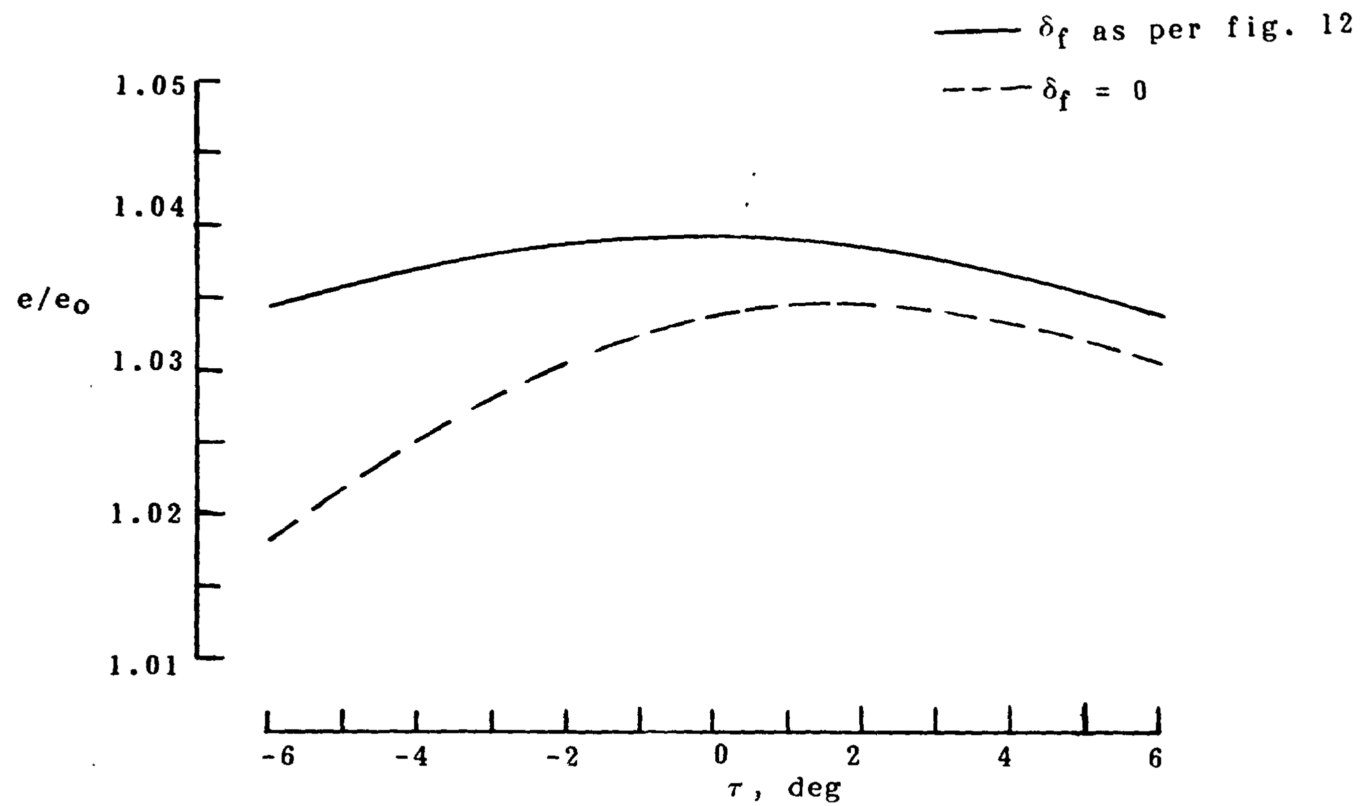

Figure 15.- Effect of vertical-fin toe angle on relative span-efficiency factor. Configuration A, $x/c = 0$, $\lambda = 0°$, $\alpha = 10°$.